Analysis of Partially Confined Blast Experiments and Simulations

Len Schwer

Schwer Engineering & Consulting Services

1. Abstract

Data and simulation results presented by Teland et al. (2018) for incident and reflected pressure histories indicated the simulation results time of arrival and pressure magnitude did not agree well with the data for the reflected shock. They posited three possibilities for the differences: (1) Charge load (explosive mass per chamber volume), (2) Afterburning and (3) Variable Gamma for the gas mixture.

The present analysis dismisses charge load and afterburning as likely causes of the simulation result differences. The focus is placed on variable gamma as the most likely cause of the observed time differences. While additional evidence is presented in support of this possibility, the lack of a variable gamma equation of state computational model for the air and detonation product mixture limits certainty.

2. Introduction

Teland et al. (2018) performed a series of explosive charge experiments inside a containment vessel attached to a long vent tube. Pressure histories were measured in the vent tube and compared to numerical results from several solvers. The goal was to assess how well the numerical simulations could replicate the second pressure pulse generated by reflections inside the containment. In general, the magnitude of the second pressure pulse is over predicted by the solvers, and the wave travels significantly faster than the data indicates.

The present manuscript attempts to demonstrate the observed time of arrival difference between the measured second pressure pulse and the numerical simulations is due to the poor representation of the detonation products by the standard JWL explosive equation of state.

3. Experimental Setup

Figure 1 illustrates the experimental setup. At the left end is the detonation chamber with an inner diameter of 162mm and 800mm length. This connects to a venting tube of internal diameter 85mm and 1200mm length. Pressure gauges are located at the left most end of the detonation chamber (P1) with two pressure gauges (P2 & P3) evenly spaced at 400mm in the venting tube. The free field incident wave gauge (P4) is positioned 1000mm from the open end of the venting tube.

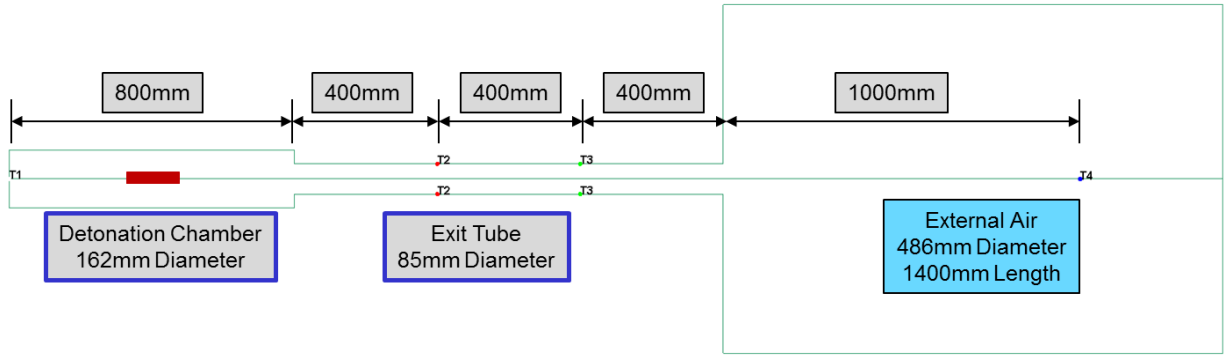

Figure 1 Schematic of test setup with location of tracer particles corresponding to pressure gauge locations.

The C-4 explosive charge is in the center of the detonation chamber and is center detonated. Table 1 lists the mass and dimensions of the four charges used in the experiments; all of charges were cylindrical with a length to diameter ratio of 5 for the three smaller charges. Two tests were performed for the three smaller charges and only one test for the largest 165gram charge[1]. The data at gauges P2 & P3 are similar differing only by time of arrival and were well replicated in the repeat tests.

Table 1 C-4 charge mass and dimensions.

Mass (grams)	Diameter (mm)	Length (mm)
20	15	4.97
41.25	19	96
82.5	24	120
165	28	176

Figure 2 shows the Teland et al. pressure history comparisons at gauge P2 for the 82.5gram C-4 charge, their Figure 11. All five simulations match[2] the time of arrival of the initial pressure pulse at about 0.2ms, although the magnitude of the initial pressures vary considerably. Of interest is the early arrival of the simulated second (reflected) pressure pulses at about 0.7ms. Of the five solvers only the one labeled CHINOOK (AB) provides a secondary pulse of approximately the correct magnitude arriving shortly before the data at 1ms. Teland et al. provided similar results for the other three charges.

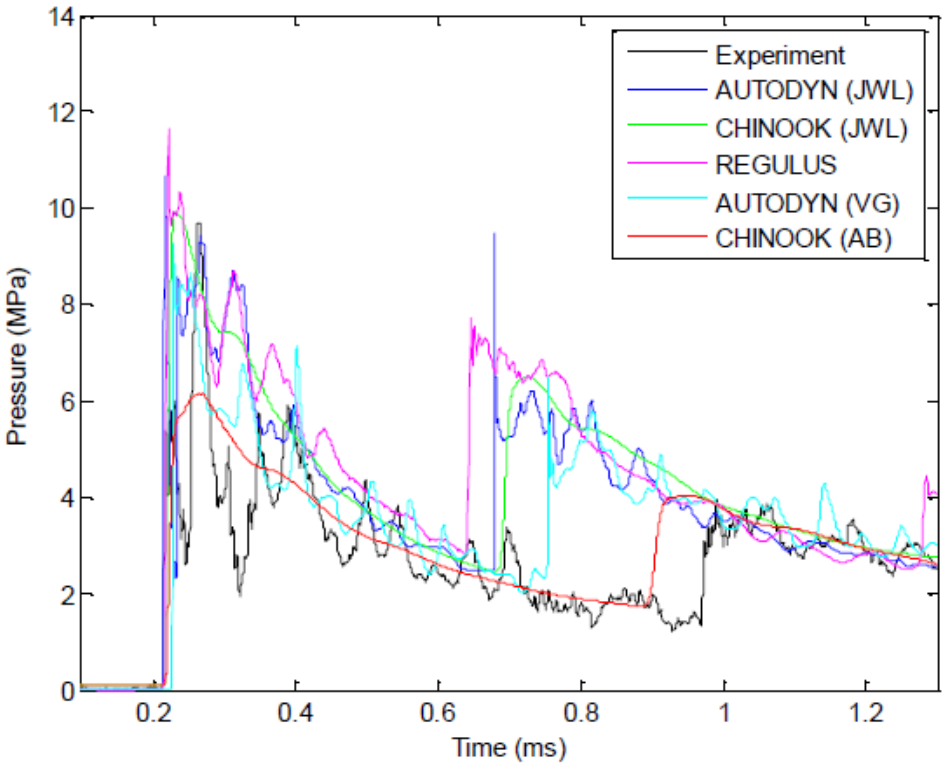

Figure 2 Pressure histories comparisons at gauge P2 for 82.5gram charge.

The reader will note that there are two results for both AUTODYN and CHINOOK shown in Figure 2. The two with the (JWL) extension used a standard Jones-Wilken-Lee equation of state for the detonation products. The AUTODYN (VG) simulation used a modified JWL EOS with a pressure dependent "variable gamma;" see Figure 6 in Teland et al. The CHINOOK result with the (AB) extension is also a variable gamma model and capable of treating afterburning (AB). Teland et al. provide the following description of this version of CHINOOK:

[1] During the present simulation of the data, it was discovered there was an error in the length measurement of the 165gram charge; the reported length of 140.4mm should have been given as 176mm.

[2] The experimental data did not have a time of detonation indicator, so the experimental results were time shifted to agree with the numerical simulation initial pressure pulse arrival times, which agreed well.

> "In CHINOOK an Afterburning / Variable Gamma (AB/VG) EOS is implemented. Here the explosive is modelled using the JWL equation of state initially, but then transits to a Variable Gamma ideal gas equation based on a density criteria [15]. The gamma calculation comes from multi-species mixture rules (based on mole fractions). For each specie, a temperature-dependent fitting equation is used (with 7 coefficients for each specie). The coefficients for each species are tabulated in textbooks and libraries such as NASA Chemical Equilibrium with Applications [16]."

Here the reference numbers refer to those in Teland et al. and are provided in this manuscript for the benefit of the reader as Donahue et al. (2013) and the URL https://www.grc.nasa.gov/www/CEAWeb/, respectively.

The observation that the AUTODYN (VG) and the CHINOOK (AB/VG) models provide an improved estimate of the second pressure wave time of arrival is a clue that how the detonation products are modeled is a possible cause of the results differences. Teland et al. also mention the possibilities that afterburning may be a contributor. Unfortunately, Teland et al. do not mention if the CHINOOK model included afterburning, nor any of the EOS input details. To address the possible effect of afterburning a LS-DYNA® simulation with afterburning will be discussed subsequently.

4. LS-DYNA Model

An axisymmetric Multi-Material Arbitrary Eulerian Lagrange (MM-ALE) model was constructed using a uniform mesh size of 2.13mm. This provides for between 7 and 13 cells across the 15 to 28mm C-4 charge diameters, respectively. This number of cells is considerably less than the "rule of thumb" recommendation of a minimum of 20 cells across the diameter of a cylindrical charge. To assess mesh sensitivity, for the smallest diameter charge, i.e. 15mm diameter of the 20g charge, a mesh using 1.14mm uniform cells was also simulated, i.e. 13 cells across the diameter. The resulting pressure histories for the two mesh refinements were essentially identical.

The external boundaries of the detonation chamber and venting tube were constrained from flow normal to the boundary. The exception was the exit end of the venting tube that was open to the adjoining free air domain. The initial and boundary condition on the air domain was one atmosphere pressure.

Constitutive and equation of state models and parameters are provided in the Appendix.

5. Laboratory Data and Simulation Results Comparisons

Of primary interest in the simulation comparisons is the arrival time and magnitude of the second pressure pulse originating from the incident blast wave reflecting off the left end of the detonation chamber. This second pressure pulse is measured at the two vent tube gauges P2 and P3. The simulations were run for 2 milliseconds to allow capture of the second pressure pulse. The pressure measurement at gauge P1 in the experiments was deemed not reliable and is ignored in the comparisons. The incident pressure measurement at P4 in the simulations was not used in the comparisons as the wave arrives close to 2 milliseconds and almost immediately reflects from the nearby one atmosphere air boundary.

In making the comparisons, the TOA for gauge P2 was adjusted to align with the TOA of tracer particle T2 at gauge location P2. This was necessary because the experiment did not include an identifiable time of detonation as a break wire could not be included in the experiment.

For brevity of the exposition, only the 82.5g C-4 charge results are discussed. As mentioned previously, all the charge results were similar; the specifics of the other charge results are presented in Teland et al.

Figure 3 compares the 82.5g C-4 charge pressure histories at gauge location P2 with the corresponding simulation results from the LS-DYNA simulation and the CHINOOK (AB/VG) results shown in Figure 11 of Teland et al. As was the case for the other four simulation results presented by Teland et al. for this charge mass, refer to previously presented Figure 2, the LS-DYNA reflected pressure pulse arrives about 0.18ms before the data and about 0.10ms before the prediction by CHINOOK (AB/VG).

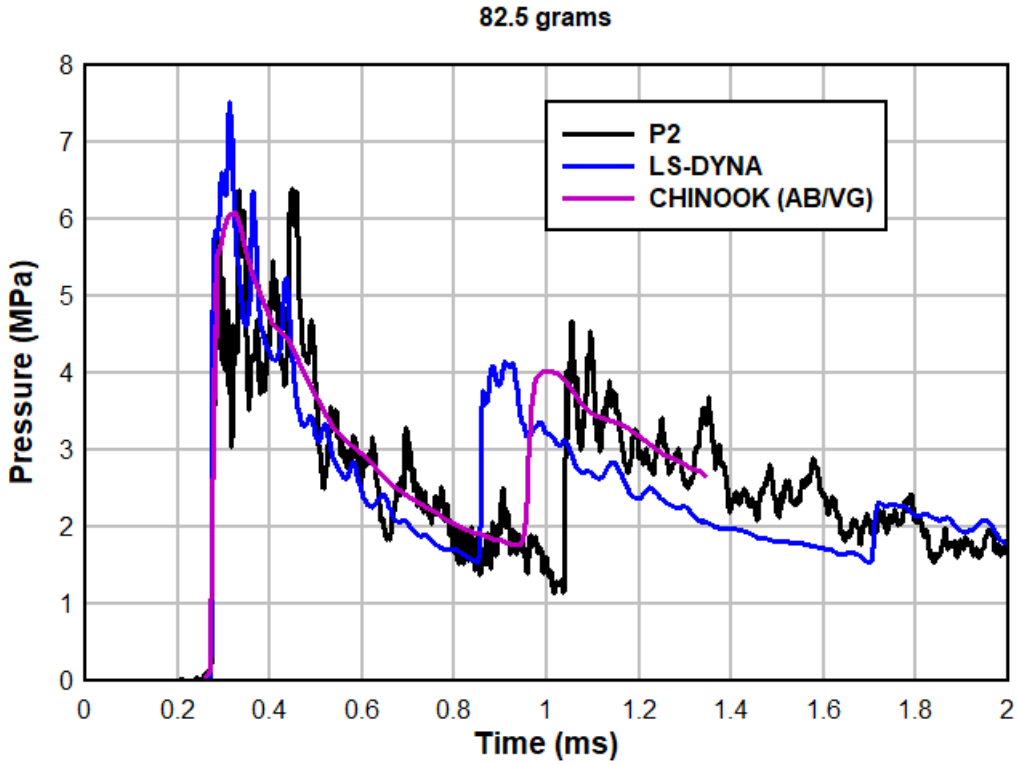

Figure 3 Comparison of pressure histories measured at gauge location P2 with the LS-DYNA and CHINOOK (AB/VG) results.

Figure 4 is an attempt to illustrated how the reflected pressure wave from the left end of the containment vessel travels through the detonation products before arriving at gauge location P2. The left side of the figure indicates the arrival of the incident wave at 0.27ms after traveling through undisturbed air, both as a fringe of pressure[3] (top) and fringe of MM-ALE materials (bottom) with the detonation products indicated by the green region.

At 0.87ms the reflected wave from the left end of the containment vessel has traveled to gauge location P2. After it reflects from the left end, the pressure wave travels through a mixture of air and detonation products out of the containment vessel and into the vent tune that also contains an air and detonation products mixture. It is this unknown mixture of air and detonation products that causes the simulated reflected wave to arrive sooner than the data indicates.

[3] The upper limit of the pressure fringe was set to 4MPa.

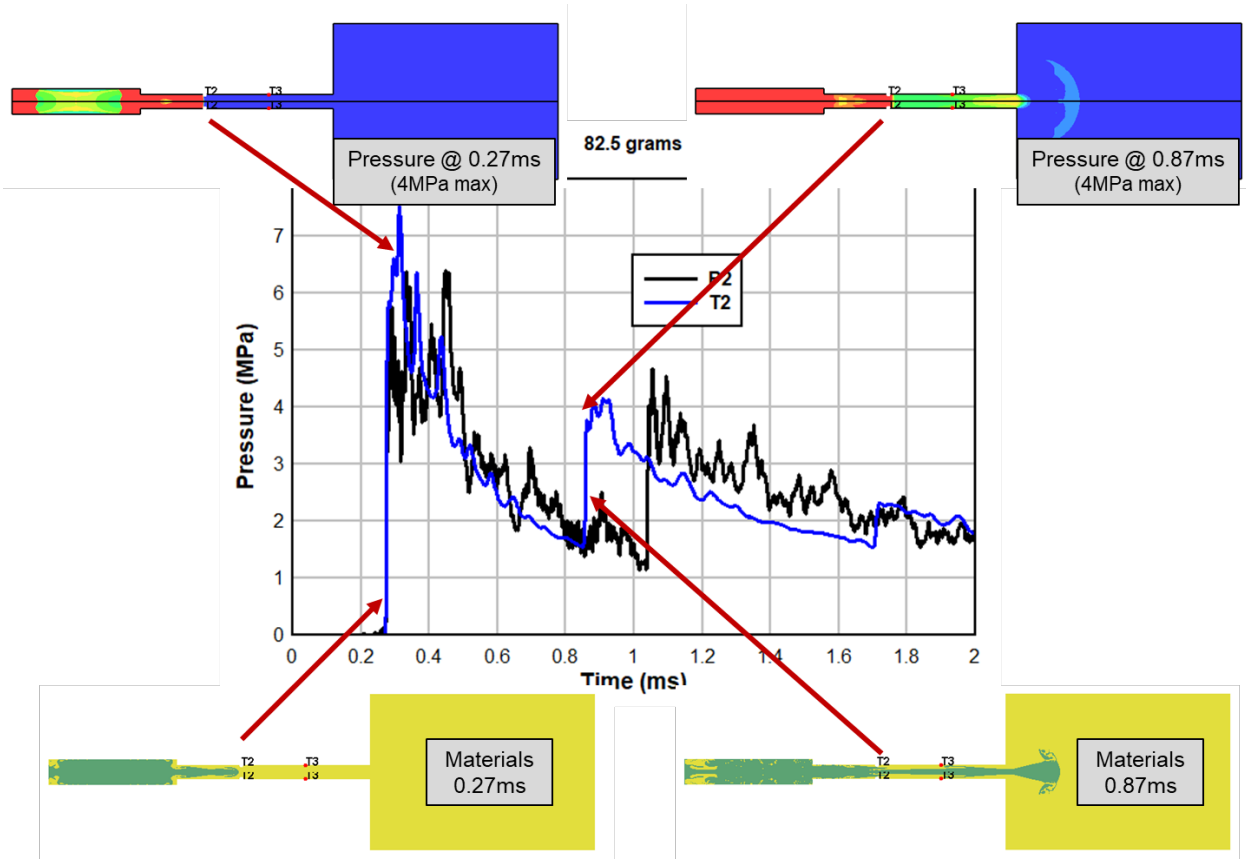

Figure 4 Annotation of LS-DYNA pressure history at gauge P2 for the 82.5g C-4 charge.

Using the simple afterburn model for the C-4 in LS-DYNA, as shown in Figure 5, leads to a worse prediction for the arrival time, i.e. earlier than without afterburning. As demonstrated by Schwer & Rigby (2017), the addition of afterburning, due to a secondary shock mixing the gases, causes the secondary shock to arrive earlier than without afterburning; the magnitude of the secondary shock is also increased due to the added afterburning energy. Figure 5 shows the effect on the pressure history of adding 9.37 GPa (6.01 MJ/kg) between 0.13 and 0.36 milliseconds for the 82.5gram C-4 charge. As indicated above, the second shock then arrives sooner with a larger magnitude.

Having addressed the question of afterburning contributing to the time of arrival of the reflected pressure wave, at least via an engineering model of afterburning, the remaining parameter is gamma. Variable gamma models were demonstrated by Teland et al. to improve the reflected wave time of arrival versus their non-variable standard JWL equivalents.

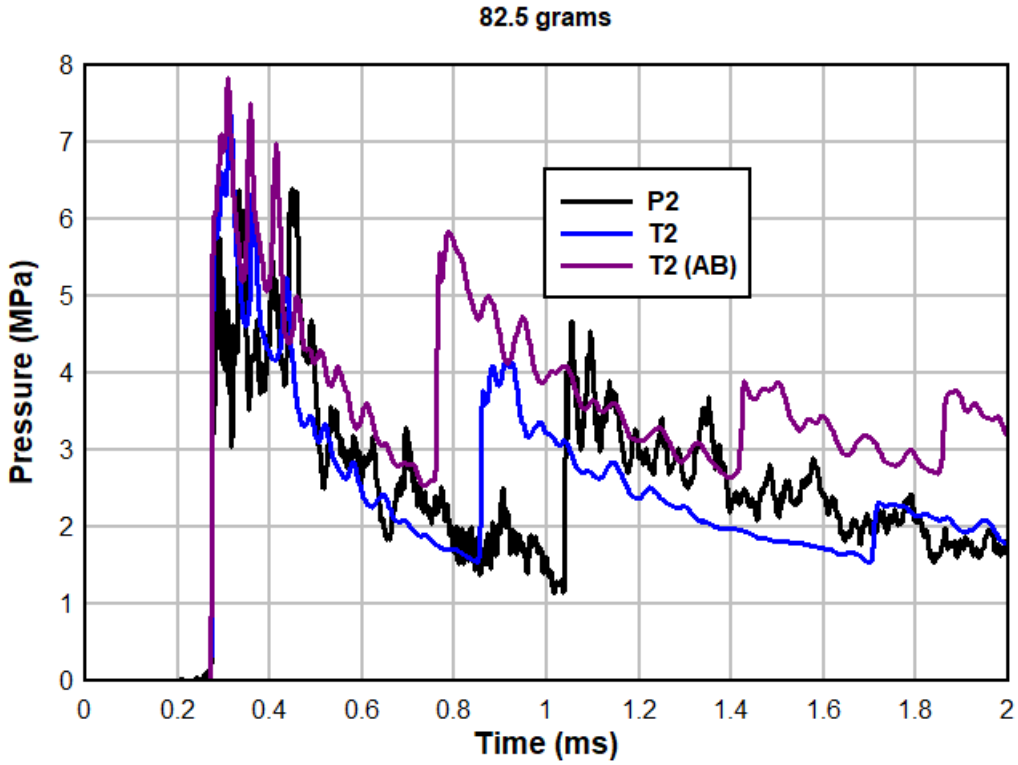

Figure 5 Comparison of LS-DYNA 82.5g C-4 pressure histories with and without afterburning.

Shock speed U can be calculated from the Hugoniot jump conditions:

$$U = C_0 \left[\frac{\Delta P}{P_0} \frac{1+\gamma}{2\gamma} + 1 \right]^{1/2} \tag{1}$$

Where C_0 is the sound speed in the gas ahead of the shock, γ is the ratio of specific heats, ΔP is the jump in pressure and P_0 is the pressure ahead of the shock. The shock speed U can be calculated from the data and the simulation using the transit time of the initial and reflected shock between the gauge locations P2 and P3 that are 400mm apart, as shown in Figure 6.

Table 2 Shock speeds U for initial and reflected waves of 82.5g C-4 charge/

	Initial Shock (m/s)	Reflected Shock (m/s)	Relative Difference
Teland et al.	2247	1951	-13%
LS-DYNA	2531	2614	3%

Table 2 compares the shock speed for the initial and reflected shock using the transit times shown in Figure 6. Given the judgement in determining these transit times, the Teland et al. data indicates the shock speed decreases by 13% between the initial and reflected shocks. While the shock speed from the LS-DYNA simulations is essentially constant.

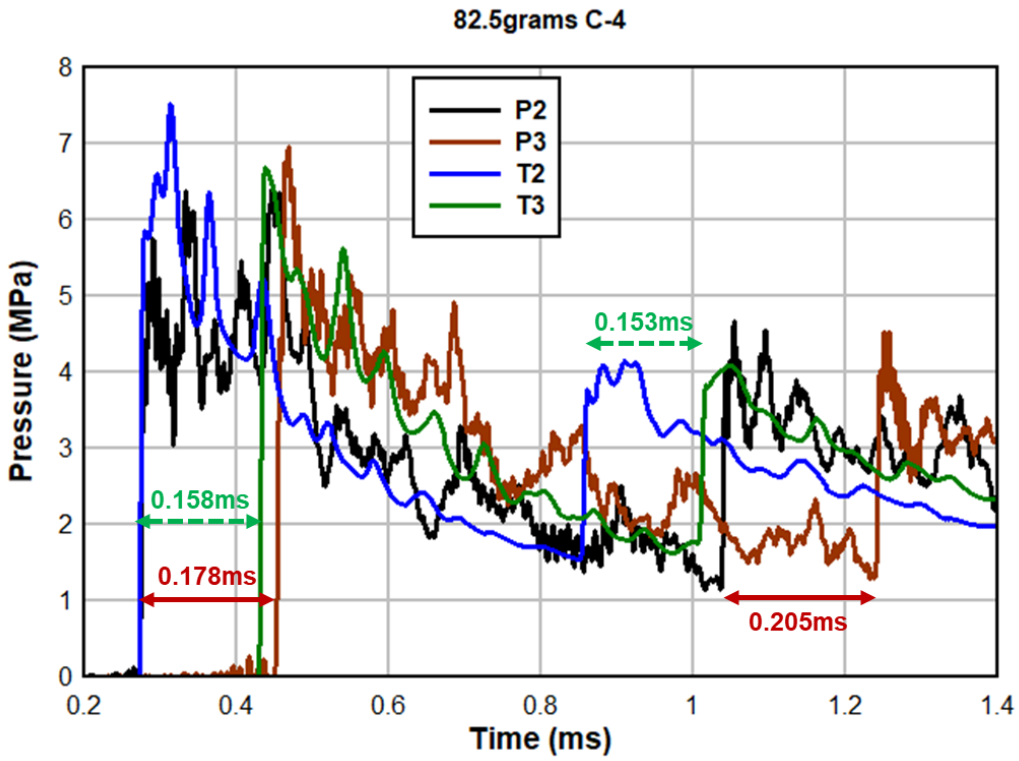

Figure 6 Wave transit times between gauge locations P2 and P3 that are 400mm apart.

In addition to the shock speed U, we can calculate the pressure increase at the shock ΔP and the pressure in the gas ahead of the shock P_0. Rewriting the above Equation (1) solving for gamma

$$\gamma = \frac{\frac{\Delta P}{P_0}}{2\left[\left(\frac{U}{C_0}\right)^2 - 1\right] - \frac{\Delta P}{P_0}} \tag{2}$$

The remaining unknown is the sound speed in the gas mixture ahead of the shock C_0. Not only is this sound speed a function of the gas mixture but also the temperature of the gas. This is the quantity CHINOOK (AB/VG) attempts to calculates as per the previously presented description:

> "The gamma calculation comes from multi-species mixture rules (based on mole fractions). For each specie, a temperature-dependent fitting equation is used (with 7 coefficients for each specie). The coefficients for each species are tabulated in textbooks and libraries such as NASA Chemical Equilibrium with Applications."

It would have been interesting if Teland et al. could have provided variable gamma histories from the CHINOOK (AB/VG) model at the two vent tube gauge locations.

$C_0 = 343$ m/s and $P_0 = 0.1$ MPa for the ambient air filling the vent tube. The initial shock speed U is taken from Table 2 and the pressure jumps are estimated as 4.53 and 5.94MPa[4] from the data and simulation results shown in

[4] The ambient pressure of 0.1MPa is added to the pressures shown in Figure 6.

Figure 6. The resulting values for gamma are 1.18 and 1.25, respectively. While these values are not the expected $\gamma = 1.4$, estimates of errors in the measured maximum pressure and time sampling of both pressure histories could account for some (all?) of the difference. For example, adding 0.4 and 0.3MPa, respectively, to the provided jump pressure results in the expected values of gamma for both cases.

6. Summary

Teland et al. (2018) presented pressure history data, and simulation results, from four C-4 charge masses at two pressure gauges located in a vent tube. The simulation comparisons indicated that the time of arrival for the reflected shock wave, reflected from the far end of the explosive containment chamber, arrive considerably earlier than indicated by the data. They proposed three possibilities for differences:

1. Charge load (explosive mass per chamber volume)
2. Afterburning
3. Variable Gamma

The charge load for the four masses varied from 1.2 to 10 kg/m^3. However, as shown in Figure 14 from Teland et al. of relative time difference (Numerical/Experimental) between initial and reflected shocks at gauge P2, this measure of time difference was essentially constant at 0.6 for all four charge masses.

A LS-DYNA simulation of the 82.5gram C-4 charge was performed including the available simple engineering model of afterburning. The addition of afterburning in this case, and others reported by Schwer & Rigby (2017), show an increase the reflected wave speed, the opposite desired effect.

Among the numerical results presented by Teland et al., two models that included a variable gamma provided better estimates of the reflected wave time of arrival when compared with the data. Of these two variable gamma models, the CHINOOK (AB/VG) model provide the best results with a relative time difference between about 0.8 and 1.0 as the charge mass increased, respectively.

Additionally, a LS-DYNA simulation without afterburning of the 82.5gram was used illustrate the path of the reflected shock from the rear of the containment chamber, through the detonation products and arriving at the two-gauge locations.

The shock speed was computed from the data and simulation results based on the transit time between the two vent tube gauges. The data indicated the shock speed decreased from the initial to reflected shock, while the simulation indicated essentially constant shock speed.

Finally, the Hugoniot jump condition equation was rewritten to show the dependence of gamma on the unknown sound speed in the gas mixture ahead of the shock. This sound speed depends on the gas mixture, air and detonation products, and the gas temperature. It is this calculation of this sound speed that apparently allows the CHINOOK (AB/VG) simulation to better agree with the data.

7. Acknowledgement

The author is grateful to Svein Christensen for sharing the digital pressure records making the pressure history comparisons possible.

8. References

Teland, J.A., K.O. Hauge, S.O. Christensen, and S. Borve, (2018), “Numerical Simulation of Confined Blast,” 25th Military Aspects of Blast and Shock (MABS) 24-28 September, Den Hague, Netherlands

Donahue L, F. Zhang, and R.C. Ripley (2013), “Numerical Models for Afterburning of TNT Detonation Products in Air,” *Shock Waves*, Volume 23, Number 6, Page 559.

Schwer, L. and S. Rigby (2017) “Reflected Secondary Shocks: Some Observations Using Afterburning,” 11th European LS-DYNA Conference, Salzburg, Austria, 9-11 May.

https://www.dynalook.com/11th-european-ls-dyna-conference/air-blast-2/secondary-shocks-and-afterburning-some-observations

9. Appendix – Constitutive and Equation of State Models

Units are grams-millimeters-milliseconds-(MPa)

Air

```
*MAT_NULL
$    MID    RO       PC    MU    TEROD   CEROD   YM   PR
     100, 1.29e-6, 0.0, 0.0, 0.0,    0.0

*EOS_Linear_Polynomial
$ EOSID  C0     C1    C2    C3    C4    C5   C6
   100 ,  0.0, 0.0, 0.0, 0.0, 0.4, 0.4, 0.0
$  e0     v0
  0.25, 1.0
```

C-4

```
*MAT_HIGH_EXPLOSIVE_BURN
$ MID     RO          D          PCJ     BETA
 1080, 1.601-3,  8.193e3,    2.8E4,   0.0

*EOS_JWL
$ EOSID      A          B       R1     R2     OMEG     E0      V0
 1080 , 6.098E5, 1.295E4,  4.5,  1.4,    0.25,  9.0E3, 1.0
```